Electronic phase transitions under hydrostatic pressure in $LaMnO_3$ (111) bilayers sandwiched between $LaAlO_3$

H. A. Tahini,[1,2] F. Cossu,[1] N. Singh,[1] S. C. Smith,[2] and U. Schwingenschlögl[1,*]

[1]*Physical Science & Engineering Division, KAUST, Thuwal 23955-6900, Kingdom of Saudi Arabia*

[2]*Integrated Materials Design Centre, School of Chemical Engineering, UNSW Australia, Sydney, NSW 2052, Australia*

(Received 12 August 2015; revised manuscript received 28 December 2015; published 13 January 2016)

Using *ab initio* calculations, we investigate the effect of hydrostatic pressure on the electronic structure of $LaMnO_3$ (111) bilayers sandwiched between $LaAlO_3$. In the ideal heterostructure we observe Dirac cones at the Fermi energy. However, octahedral tiltings open a band gap and thus destroy the Dirac nature. We show that the effect of the tiltings can be suppressed by hydrostatic pressure from 40 GPa to 60 GPa. At higher pressure further phase transitions are encountered.

DOI: 10.1103/PhysRevB.93.035117

Every now and then transition metal oxides reveal new mysteries and fascinating properties [1–5]. Merging two or more of these compounds can lead to functionalities that are lacking in each individual oxide. An example is the two-dimensional electron gas formed at the interface between $LaAlO_3$ and $SrTiO_3$ [6] or the possible superconductivity at the interface between $LaNiO_3$ and $LaMnO_3$ [7]. More recently, by considering growth orientations other than (001), additional exotic properties have been predicted, such as the existence of a tunable topological band structure for transition metal oxide bilayers, which can host a quantum spin Hall effect [8], for example. Topological phases indeed have been theorized to emerge in e_g systems such as $LaNiO_3$ (111) [9], $LaNiO_3/LaAlO_3$ (111) interface [10–12], and $LaAuO_3$[13]. The $LaAlO_3/SrTiO_3$ heterostructure is another example for a strong interplay between the electronic and lattice degrees of freedom that leads to rich phenomena from Dirac to charge-ordered multiferroic phases [14]. Very recently, Weng *et al.* [15] have used tight binding and first principles calculations to show that $LaMnO_3$ bilayers can form a magnetic topological insulator. Similar findings have been reported in Ref. [16].

Still, there remain key challenges in perovskite oxide (111) superlattices. A first issue are difficulties in the growth due to the highly charged atomic layers encountered in this direction (strong tendency of polar surfaces to structural reconstruction). However, there have been important experimental breakthroughs in recent years in this respect, achieving better control of the atomic assembling [17–19]. Another very critical issue is the prominent role of octahedral tiltings, which can be present already in the parent compounds but typically are significantly enhanced at the interfaces in superlattices, partially to alleviate the lattice mismatch between the component materials. From a theoretical point of view, it is essential to take into account these effects in order to correctly describe the electronic properties [17].

In this work we study the $LaMnO_3/LaAlO_3$ (111) superlattice and demonstrate the existence of Dirac states at the Fermi energy, which are perturbed by strong octahedral tiltings, as manifested by a large band gap. Importantly, we find that it is possible to control the size of the band gap by applying hydrostatic pressure. Earlier work indeed has demonstrated an insulator-to-metal transition for $LaMnO_3$ at a pressure of about 32 GPa [20] along with a quenching of Jahn-Teller distortions. Our results show that hydrostatic pressure also provides a viable route for tuning the electronic structure of perovskite oxide (111) superlattices. In particular, under pressure the Dirac states of the $LaMnO_3/LaAlO_3$ (111) superlattice become accessible for further study and possible application in electronic devices.

Our calculations employ density functional theory as implemented in the Vienna *Ab initio* Simulation Package [21], the Perdew-Burke-Ernzerhof flavor of the generalized gradient approximation for the exchange correlation functional, and pseudopotentials generated from projector augmented wave functions with La $4s^2 4p^6 5s^2 6d^1$, Al $3s^2\,3p^1$, Mn $3s^2\,3p^6\,4s^2\,3d^5$, and O $2s^2 2p^4$ valence states. Electronic correlation effects are modeled by onsite corrections ($U = 4$ eV and $J = 1$ eV) for the Mn $3d$ states [22]. The energy and forces are converged with tolerances of 10^{-5} eV and 0.01 eV/Å, respectively. Plane waves with a kinetic energy cutoff of 400 eV are used and the Brillouin zone is sampled on a Γ-centered $6 \times 6 \times 2$ grid, which is refined to $12 \times 12 \times 2$ for calculating the density of states (DOS). Moreover, in the band structure calculations each high symmetry path is sampled on 100 points. Hydrostatic pressure is applied to the system by setting the stress tensor to the desired pressure and then allowing the system to fully relax, which generates a (p, V, E) data point. To validate this approach, we use the Birch-Murnaghan equations of state [23], which links the pressure p and energy E to the cell volume V, to fit our *ab initio* results and calculate B_0 and B_0'. The two methods are found to agree convincingly well. We note that treating highly correlated systems is not adequate with standard DFT. While the inclusion of an onsite U parameter can lead to an improvement in describing localized electrons, the method could still fail in classifying topological phases or metal-insulator transitions. For instance, previous DFT calculations [24] have predicted that $SrIrO_3$ bilayers would exhibit topological properties, whereas, DFT+DMFT (dynamical mean-field theory) predicted an AFM insulator [13], which is in a better agreement with recent experimental work [19]. On the other hand, Yamasaki *et al.* [25] have used LDA + U and LDA+DMFT to study the properties of bulk $LaMnO_3$ under pressure yielding consistent results for the

*udo.schwingenschlogl@kaust.edu.sa

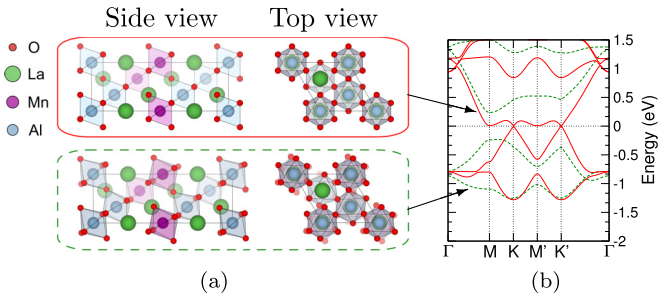

FIG. 1. (a) Structure at ambient pressure without (top) and with (bottom) octahedral tiltings. (b) Corresponding band structures. Red (solid) lines represent the superlattice without tiltings and green (dashed) lines that with tiltings. Only the spin-up bands are shown.

two methods. This is due to the robustness of the magnetic ordering in Mn-based systems which enables DFT + U to reasonably describe the electronic and magnetic evolution with pressure.

Figure 1 shows for the superlattice without tiltings of the O octahedra Dirac states close to the Fermi energy at the K and K' points. However, it turns out that this structure has not the lowest energy. By allowing structural relaxation, octahedral tiltings develop and the energy is lowered by 0.45 eV per formula unit. The resulting low energy structure is semiconducting with a band gap of about 0.5 eV and should be observed experimentally rather than the Dirac states. Middey and coworkers recently have succeeded in growing $LaNiO_3$/$LaAlO_3$ (111) superlattices [17]. However, contrary to theoretical predictions of a metallic behavior [11,12], they found an insulating phase. The importance of structural relaxations for the opening of a band gap has been stressed by the authors of Ref. [26]. In order to tune the electronic states, in particular the band gap and dispersion near the Fermi energy, hydrostatic pressure can be an efficient tool, as has been shown previously for comparable systems; see, for example, Refs. [27–29]. Hydrostatic pressure is also known to straighten the metal-O-metal bonds in perovskite oxides and alleviate octahedral tiltings [30].

We obtain superlattice parameters of $a,b = 5.41$ Å and $c = 13.33$ Å, which lie between the values of bulk $LaMnO_3$ and $LaAlO_3$, as shown in Table I. The c/a ratio of 2.46 under ambient pressure drops slightly to 2.45 at 100 GPa and thus remains close to the ideal value of $\sqrt{6}$. At 0 GPa the Mn-O-Mn angles are close to 160° [see Fig. 2(a)]. Under pressure they increase (179° at 100 GPa) to yield almost linear Mn-O-Mn bonds. Neighboring O octahedra are tilted out of phase reminiscent of the $a^-a^-a^-$ pattern of the bulk compounds with $R\bar{3}c$ symmetry. However, the tilting is characterized by different magnitudes for the MnO_6 and AlO_6 octahedra, which can be attributed to their different sizes. We observe also a quenching of the Jahn-Teller distortion [see Fig. 2(b)], as quantified by the Q_2 and Q_3 parameters [35]. Both parameters change significantly up to a pressure of 40 GPa and then remain almost constant up to about 70 GPa. At higher pressure the Jahn-Teller distortion disappears.

TABLE I. Lattice parameters and band gap of the superlattice at ambient pressure. The corresponding properties of the parent compounds are given for comparison.

	a,b (Å)	c (Å)	V_0 (Å)	E_g (eV)
Superlattice	5.41	13.33	337	0.5
$LaMnO_3$	5.52 [31]	13.32 [31]	352 [31]	1.7 [32]
$LaAlO_3$	5.37 [33]	13.14 [33]	328 [33]	5.6 [34]

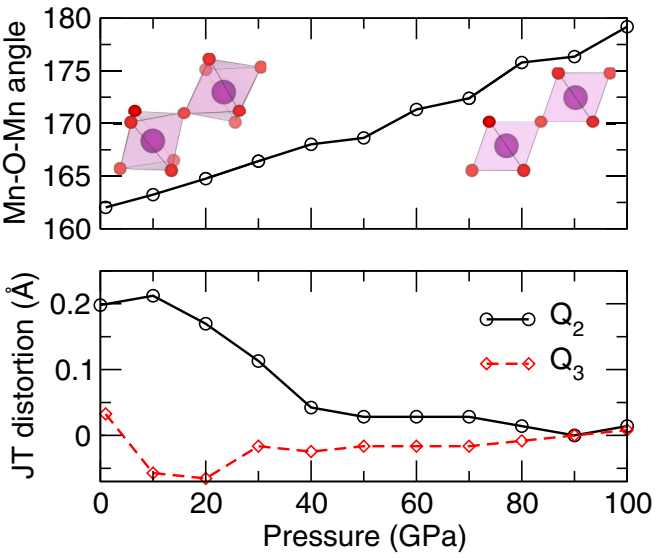

FIG. 2. (a) Octahedral tilting and (b) Jahn-Teller distortion as functions of the hydrostatic pressure.

All Mn magnetic moments are the same and we find no charge disproportionation in the considered pressure range, in contrast to bulk $LaMnO_3$ [36]. Being also an e_g^1 system, the $LaNiO_3$/$LaAlO_3$ superlattice likewise is predicted to exhibit charge disproportionation with breathing distortions of the NiO_6 octahedra [26]. Examining the local environments of the Mn atoms in our case, we find that under ambient pressure the average Mn-O bond length is 1.98 Å and the volume of the O octahedron is 10.3 Å^3. Figure 3(a) shows the variation in the Mn magnetic moments with pressure. At 0 GPa we obtain 3.6 μ_B, which remains fairly constant up to 80 GPa (i.e., 78% of the original volume). The exhibited ferromagnetism is at variance with the properties of bulk $LaMnO_3$, which is an A-type antiferromagnet ($\Delta_{FM-AFM_A} \sim 0.08$ eV per Mn ion). This ferromagnetic ordering can be explained based on the observed orbital ordering [see Fig. 3(c)], since the orbitals $d_{3x^2-r^2}$ and $d_{3y^2-r^2}$ can be assigned to Mn1 and Mn2, respectively. This gives rise to a situation analogous to undoped $LaMnO_3$, where in-plane ferromagnetism is obtained on the basis of cooperative Jahn Teller distortions [37] (hopping between nonoverlapping O p and Mn2 d orbitals is negligible according to a Slater-Koster integral evaluation [38]). Calculations with a $2 \times 1 \times 1$ supercell containing two Mn ions per layer also have been performed to test for various antiferromagnetic orderings. We find that ferromagnetism at 0 GPa is lower in energy than A-, C-, and G-type antiferromagnetism by 0.23 eV, 0.25 eV, and 0.21 eV per Mn ion, respectively. The preference for ferromagnetism

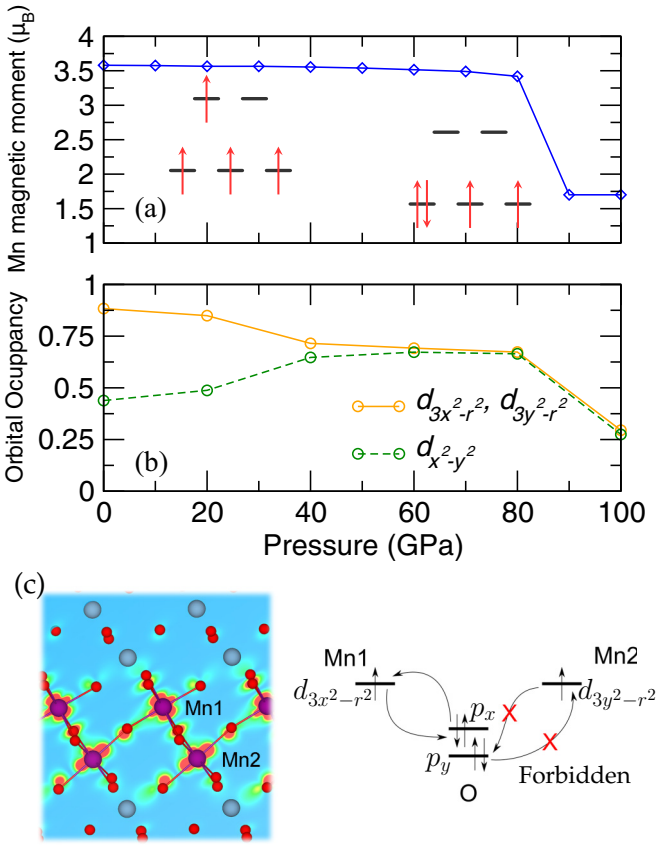

FIG. 3. (a) Mn magnetic moment and (b) occupation of the $d_{3z^2-r^2}$ and $d_{x^2-y^2}$ orbitals as functions of the hydrostatic pressure. (c) Slice through the charge density of the Mn occupied bands showing an orbitally ordered pattern. Interactions are mediated by O, giving rise to a ferromagnetic coupling.

persists under pressure but the energy difference to antiferromagnetism decreases ($\Delta_{\mathrm{FM-AFM_G}} \sim 0.10$ eV per Mn ion at 40 GPa).

For pressure beyond 80 GPa, the magnetic moments drop to 1.7 μ_B, reflecting a transition from a high ($t_{2g}^3\ e_g^1$) to a low ($t_{2g}^4\ e_g^0$) spin state. The same behavior has been predicted for bulk $LaMnO_3$ [39]. Both in bulk $LaMnO_3$ and in our case the magnetic moments start to collapse as the Mn-O-Mn angles approach 180° and the Jahn-Teller distortion is quenched.

The Jahn-Teller distortion lifts the degeneracy of the $d_{3z^2-r^2}$ and $d_{x^2-y^2}$ states. More specifically, the calculated orbital

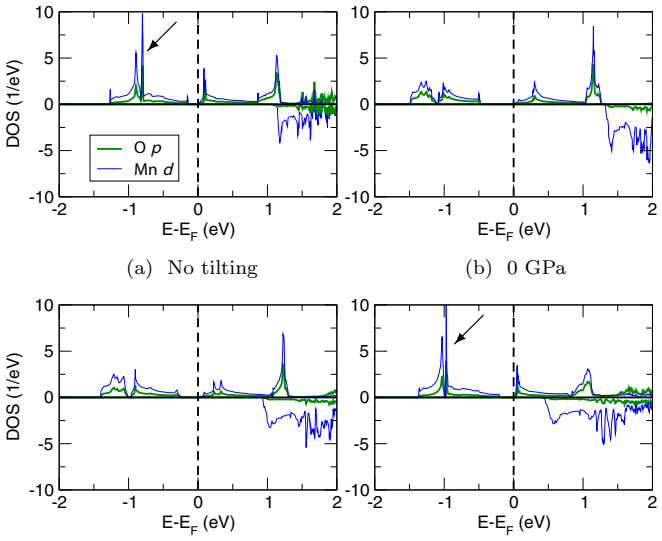

FIG. 5. Density of states. (a) 0 GPa without octahedral tilting, (b) 0 GPa with octahedral tilting, (c) 20 GPa, and (d) 40 GPa.

occupancies in Fig. 3(b) indicate a preference to fill the $d_{3z^2-r^2}$ states at low pressure when the Jahn-Teller distortion is most pronounced. At 0 GPa the orbital polarization [40],

$$\mathcal{P} = (n_{3z^2-r^2} - n_{x^2-y^2})/(n_{3z^2-r^2} + n_{x^2-y^2}), \qquad (1)$$

is 34%. As the pressure increases the $d_{3x^2-r^2}/d_{3y^2-r^2}$ occupancy begins to drop and at the same time the $d_{x^2-y^2}$ occupancy grows, until degeneracy is restored near 80 GPa. With the transition from high to low spin both orbitals become empty at higher pressure.

To shed additional light on the electronic properties, we show in Fig. 4 band structures along the path Γ-M-K-M′-K′-Γ. This choice allows us to elucidate effects of the tetragonal Jahn-Teller distortion, which lifts the equivalency of the M and M′ (K and K′) points. At 0 GPa and without octahedral tiltings [see Fig. 1(b)], the bands show a dispersion of about 0.8 eV along the path M-K-M′-K′, reflecting covalent bonding. Tiltings result in a significant reduction of the dispersion to about 0.4 eV along with the disappearance of the Dirac cones at the K and K′ points. This situation persists up to 20 GPa, where the main features of the 0-GPa band structure are recovered, except for a smaller band gap of about 0.2 eV.

Fundamental changes are encountered as the pressure is increased to 40 GPa ($V/V_0 = 0.87$), which is the point where the

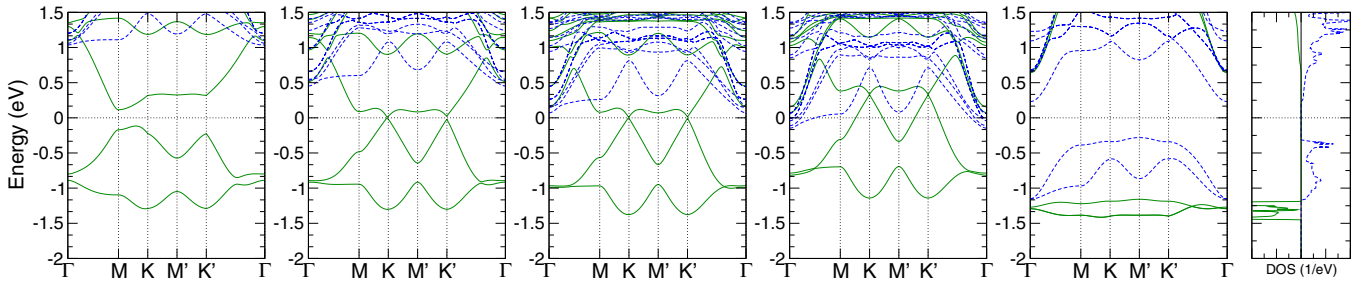

FIG. 4. Band structure evolution with pressure. The green (solid) and blue (dashed) lines represent spin-up and spin-down, respectively.

Jahn-Teller distortion is largely suppressed [see Fig. 2(b)]. The results resemble the 0-GPa band structure without octahedral tiltings. However, due to the broken inversion symmetry, small band gaps of different size open at the K and K′ points (10 meV and 50 meV, respectively). At 60 GPa the band structure remains qualitatively unchanged even though the volume has shrunk to 82% of the original value. This is expected from Fig. 2(b) as the Jahn-Teller distortion remains essentially constant for volumes in this range. A metallic behavior emerges at 80 GPa due to almost rigid shifts of bands below and above the Fermi energy. Because the Dirac cones are no longer pinned to the Fermi energy, no special behavior of the material is expected. When we approach 100 GPa the band structure reflects a transition from high to low spin, as manifested by the Mn magnetic moments. The dispersing e_g band vanishes and two bands appear that correspond to the electrons transferred to the spin-down channel.

The above discussion indicates that the absence of octahedral tiltings by itself is not sufficient to establish a linear dispersion. Even at 40 GPa (onset of the Dirac states) the Mn-O-Mn angle is 167°. In general, an angle approaching 180° implies an enhanced overlap between the Mn 3*d* and O 2*p* orbitals. This can be seen in Fig. 5(a), as the occupied states in the vicinity of the Fermi energy are strongly hybridized (indicated by an arrow). Remarkably, at 40 GPa the same kind of hybridization of the Mn 3*d* and O 2*p* states is observed [see Fig. 5(d)], but neither at 0 GPa with octahedral tiltings nor at 20 GPa.

In conclusion, we have studied the electronic structure of $LaMnO_3$ bilayers sandwiched between $LaAlO_3$. The buckled honeycomb structure of $LaMnO_3$ generates Dirac states that can be tuned by the application of pressure. A series of electronic transitions is predicted including both insulating and metallic phases. This intimate interplay between the lattice and electronic degrees of freedom together with the specific geometry of perovskite oxide (111) bilayers and a multitude of possible ionic combinations opens an unprecedented playground in the field of Dirac systems.

F.C. would like to thank Dr Yaroslav Kvashnin for useful discussions. Research reported in this publication was supported by the King Abdullah University of Science and Technology (KAUST). Additional support was provided by the Pawsey Supercomputing Centre with funding from the Australian Government and the Government of Western Australia.

[1] H. Hwang, Y. Iwasa, M. Kawasaki, B. Keimer, N. Nagaosa, and Y. Tokura, Nat. Mater. **11**, 103 (2012).
[2] J. Chakhalian, A. Millis, and J. Rondinelli, Nat. Mater. **11**, 92 (2012).
[3] P. Yu, Y.-H. Chu, and R. Ramesh, Materials Today **15**, 320 (2012).
[4] F. M. Granozio, G. Koster, and G. Rijnders, MRS Bull. **38**, 1017 (2013).
[5] L. Bjaalie, B. Himmetoglu, L. Weston, A. Janotti, and C. G. Van de Walle, New J. Phys. **16**, 025005 (2014).
[6] A. Ohtomo and H. Hwang, Nature (London) **427**, 423 (2004).
[7] J. C. V. Chaloupka and G. Khaliullin, Phys. Rev. Lett. **100**, 016404 (2008).
[8] D. Xiao, W. Zhu, Y. Ran, N. Nagaosa, and S. Okamoto, Nat. Commun. **2**, 596 (2011).
[9] K.-Y. Yang, W. Zhu, D. Xiao, S. Okamoto, Z. Wang, and Y. Ran, Phys. Rev. B **84**, 201104 (2011).
[10] A. Rüegg and G. A. Fiete, Phys. Rev. B **84**, 201103 (2011).
[11] A. Rüegg, C. Mitra, A. A. Demkov, and G. A. Fiete, Phys. Rev. B **85**, 245131 (2012).
[12] A. Rüegg, C. Mitra, A. A. Demkov, and G. A. Fiete, Phys. Rev. B **88**, 115146 (2013).
[13] S. Okamoto, W. Zhu, Y. Nomura, R. Arita, D. Xiao, and N. Nagaosa, Phys. Rev. B **89**, 195121 (2014).
[14] D. Doennig, W. E. Pickett, and R. Pentcheva, Phys. Rev. Lett. **111**, 126804 (2013).
[15] Y. Weng, X. Huang, Y. Yao, and S. Dong, Phys. Rev. B **92**, 195114 (2015).
[16] D. Doennig, S. Baidya, W. E. Pickett, and R. Pentcheva, arXiv:1510.09177.
[17] S. Middey, D. Meyers, M. Kareev, E. J. Moon, B. A. Gray, X. Liu, J. W. Freeland, and J. Chakhalian, Appl. Phys. Lett. **101**, 261602 (2012).
[18] I. Hallsteinsen, J. E. Boschker, M. Nord, S. Lee, M. Rzchowski, P. E. Vullum, J. K. Grepstad, R. Holmestad, C. B. Eom, and T. Tybell, J. Appl. Phys. **113**, 183512 (2013).
[19] D. Hirai, J. Matsuno, and H. Takagi, APL Materials **3**, 041508 (2015).
[20] I. Loa, P. Adler, A. Grzechnik, K. Syassen, U. Schwarz, M. Hanfland, G. K. Rozenberg, P. Gorodetsky, and M. P. Pasternak, Phys. Rev. Lett. **87**, 125501 (2001).
[21] G. Kresse and D. Joubert, Phys. Rev. B **59**, 1758 (1999).
[22] A. I. Liechtenstein, V. I. Anisimov, and J. Zaanen, Phys. Rev. B **52**, R5467 (1995).
[23] F. Birch, Phys. Rev. **71**, 809 (1947).
[24] J. L. Lado, V. Pardo, and D. Baldomir, Phys. Rev. B **88**, 155119 (2013).
[25] A. Yamasaki, M. Feldbacher, Y.-F. Yang, O. K. Andersen, and K. Held, Phys. Rev. Lett. **96**, 166401 (2006).
[26] D. Doennig, W. E. Pickett, and R. Pentcheva, Phys. Rev. B **89**, 121110 (2014).
[27] V. Laukhin, J. Fontcuberta, J. L. García-Muñoz, and X. Obradors, Phys. Rev. B **56**, R10009 (1997).
[28] R. Søndenå, P. Ravindran, S. Stølen, T. Grande, and M. Hanfland, Phys. Rev. B **74**, 144102 (2006).
[29] H. J. Zhao, X. Q. Liu, X. M. Chen, and L. Bellaiche, Phys. Rev. B **90**, 195147 (2014).
[30] B. Magyari-Köpe, L. Vitos, B. Johansson, and J. Kollár, Phys. Rev. B **66**, 092103 (2002).
[31] Q. Huang, A. Santoro, J. W. Lynn, R. W. Erwin, J. A. Borchers, J. L. Peng, and R. L. Greene, Phys. Rev. B **55**, 14987 (1997).
[32] T. Saitoh, A. E. Bocquet, T. Mizokawa, H. Namatame, A. Fujimori, M. Abbate, Y. Takeda, and M. Takano, Phys. Rev. B **51**, 13942 (1995).
[33] X. Luo and B. Wang, J. Appl. Phys. **104**, 073518 (2008).

[34] S.-G. Lim, S. Kriventsov, T. N. Jackson, J. H. Haeni, D. G. Schlom, A. M. Balbashov, R. Uecker, P. Reiche, J. L. Freeouf, and G. Lucovsky, J. Appl. Phys. **91**, 4500 (2002).
[35] K. I. Kugel' and D. I. Khomskiĭ, Sov. Phys. Usp. **25**, 231 (1982).
[36] G. Banach and W. M. Temmerman, J. Phys.: Condens. Matter **16**, S5633 (2004).
[37] M. Capone, D. Feinberg, and M. Grilli, J. Phys. IV **09**, PR10-335 (1999).
[38] J. C. Slater and G. F. Koster, Phys. Rev. **94**, 1498 (1954).
[39] J. He, M.-X. Chen, X.-Q. Chen, and C. Franchini, Phys. Rev. B **85**, 195135 (2012).
[40] M. J. Han, C. A. Marianetti, and A. J. Millis, Phys. Rev. B **82**, 134408 (2010).